



# A novel fluorescent chemosensor based on coumarin and quinolinyl-benzothiazole for sequential recognition of Cu<sup>2+</sup> and PPI and its applicability in live cell imaging

Shengling Li<sup>a</sup>, Duanlin Cao<sup>a</sup>, Xianjiao Meng<sup>c</sup>, Zhiyong Hu<sup>a,b</sup>, Zhichun Li<sup>a</sup>, Changchun Yuan<sup>a</sup>, Tao Zhou<sup>a</sup>, Xinghua Han<sup>a,b</sup>, Wenbing Ma<sup>a,b,\*</sup>

<sup>a</sup> School of Chemical Engineering and Technology, North University of China, Taiyuan 030051, PR China

<sup>b</sup> National Demonstration Center for Experimental Comprehensive Chemical Engineering Education, North University of China, Taiyuan 030051, PR China

<sup>c</sup> College of Arts and Sciences, Shanxi Agricultural University, Taiyuan, Shanxi 030801, PR China

## ARTICLE INFO

### Article history:

Received 6 November 2019

Received in revised form 24 December 2019

Accepted 30 December 2019

Available online 03 January 2020

### Keywords:

Coumarin

Sequential recognition

Fluorescent sensor

Cu<sup>2+</sup>

PPI

## ABSTRACT

In this study, a highly selective fluorescent sensor (*E*)-2-((2-(benzo[d]thiazol-2-yl)quinolin-8-yl)oxy)-*N'*-((7-(diethylamino)-2-oxo-2*H*-chromen-3-yl)methylene)acetohydrazide (**TQC**) was synthesized from 2-methylquinolin-8-ol and 4-(diethylamino)-2-hydroxybenzaldehyde and its structure was characterized by <sup>1</sup>H NMR, <sup>13</sup>C NMR, ESI-HR-MS and density functional theory (DFT) calculation. Sensor **TQC** showed an obvious “on-off-on” fluorescence response to Cu<sup>2+</sup> and PPI in a DMSO/HEPES (3:2 v/v, pH = 7.4) buffer system. The detection limits of sensor **TQC** were 0.06 μM to Cu<sup>2+</sup> and 0.01 μM to PPI. In addition, sensor **TQC** showed a 1:1 binding stoichiometry to Cu<sup>2+</sup> and **TQC**-Cu<sup>2+</sup> complex showed a 2:1 binding stoichiometry to PPI. The optimum pH range of sensor **TQC** and **TQC**-Cu<sup>2+</sup> was 3–8. Further studies demonstrated that sensor **TQC** could be made into test paper strips for the qualitative of Cu<sup>2+</sup> and PPI and showed sequentially “on-off-on” fluorescent bio-imaging of Cu<sup>2+</sup> and PPI in HeLa cells.

© 2020 Elsevier B.V. All rights reserved.

## 1. Introduction

As is known to all, fluorescent sensors can be utilized as an effective tool for detection ions on the basis of their high selectivity and high sensitivity [1–3]. Furthermore, sensors of sequential recognition of cations and anions have caused more attention to do extensive research, and dozens of fluorescent sensors have been reported, such as Zn<sup>2+</sup>/PPI [4,5], Al<sup>3+</sup>/PPI [6–8], Al<sup>3+</sup>/H<sub>2</sub>PO<sub>4</sub><sup>-</sup>/CN<sup>-</sup> [9], Fe<sup>3+</sup>/PPI [10–12], Cu<sup>2+</sup>/PPI [13–15], Ag<sup>+</sup>/F<sup>-</sup> [16], Hg<sup>2+</sup>/S<sup>2-</sup> [17–18] and so on.

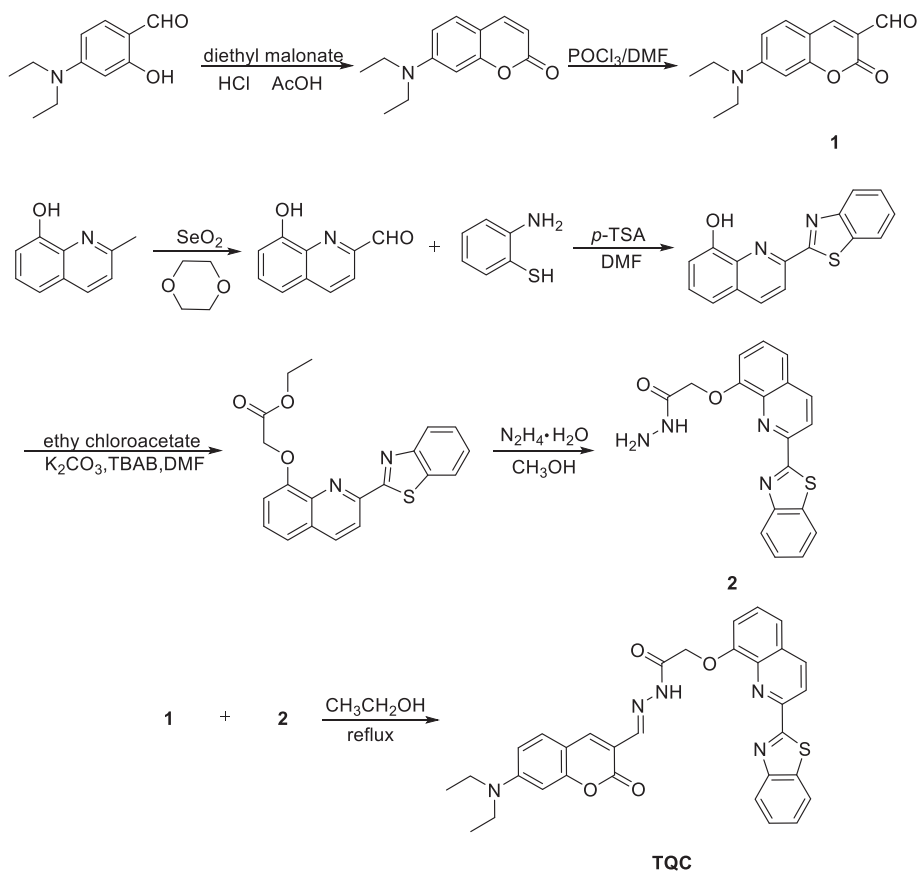
Cu<sup>2+</sup> is an essential element in human body and moderate concentration of Cu<sup>2+</sup> is of great benefit to maintain the normal function of body [19–21]. The data shows that the allowable limits of Cu<sup>2+</sup> are 1.3 ppm (20 μM) [22] in drinking water and 15.7–23.6 μM [23] in blood. Higher or lower concentration of Cu<sup>2+</sup> can seriously interfere with normal physiological activities which leads to various diseases [24–26]. Therefore, it is vital to detect Cu<sup>2+</sup> and track its role in life activities. So far, the types of sensor that identify in relation to Cu<sup>2+</sup> sequentially are Cu<sup>2+</sup>/PPI [13–15], Cu<sup>2+</sup>/S<sup>2-</sup> [27–30], Cu<sup>2+</sup>/H<sub>2</sub>PO<sub>4</sub><sup>-</sup> [22,31], and Cu<sup>2+</sup>/F<sup>-</sup> [32].

PPI is the hydrolysis product of adenosine triphosphate in living cells, and it has many important biological functions and is involved in many energy conversions and metabolic processes [33–35]. A stable metabolic process allows for the normal functioning of the organism [36–38]. However, there often exist many phosphorus-containing anions with the same charge and similar structure in the body, making it very difficult to selectively identify PPI from various phosphoric acid derivatives. Using a specific Cu<sup>2+</sup> sensor to sequentially identify PPI which can effectively eliminate the interference of other quenching agents in the system on Cu<sup>2+</sup> would be more cost-effective and convenient [39] (Scheme 1).

Coumarin fluorophores are often applied in structural design of fluorescent dyes due to their advantages of high fluorescence quantum yield, large Stokes shift and superior light stability [40] and the nitrogen and oxygen atoms in benzothiazole and quinoline have excellent coordination ability to metal ions [41–44]. In this paper, we synthesized a new fluorescent sensor **TQC** based on coumarin and quinolinyl-benzothiazole which showed an obvious “on-off” fluorescence quenching response toward Cu<sup>2+</sup> with a quenching efficiency of 100%, and **TQC**-Cu<sup>2+</sup> complex showed an “off-on” fluorescence enhancement response toward PPI in a DMSO/HEPES (3:2 v/v, pH = 7.4). It showed higher selectivity, higher sensitivity than current fluorescent sensors in sequential recognition of Cu<sup>2+</sup> and PPI.

\* Corresponding author at: School of Chemical Engineering and Technology, North University of China, Taiyuan 030051, PR China.

E-mail address: [mawenbing@nuc.edu.cn](mailto:mawenbing@nuc.edu.cn) (W. Ma).



Scheme 1. Synthesis of sensor molecule TQC

## 2. Experimental

### 2.1. Materials and methods

Compounds **1** and **2** were synthesized according to the reported reference. [45, 46] The raw material was purchased from Aladdin and Energy Chemical Reagents Ltd. All solvents were commercially available AR and CP and were used without any treatment. The <sup>1</sup>H NMR and <sup>13</sup>C NMR spectra were measured on a Bruker AVANCE III spectrometer (Switzerland) in CDCl<sub>3</sub> solution at 400 and 100 MHz, respectively. The ESI-MS spectra of sensor TQC was measured on a Bruker Solarix XR Fourier transform-ion cyclotron resonance (FT-ICR) mass spectrometer. The UV-spectra and fluorescence spectra of all samples were recorded on a UV-2602 spectrophotometer and HITACHI-F-2700 spectrophotometer. Transient photoluminescence decay spectra were recorded on Edinburgh FLS1000 steady-state/transient fluorescence spectrometer. The melting points of sensor TQC was obtained on a WRS-C1 microcomputer melting point instrument. The pH of all solutions was making-up on a PHS-3C pH meter. The bright field, fluorescence and confocal fluorescence microscope images of the cells were obtained using a fluorescence microscope (EVOS fl auto, life, America) at an excitation wavelength of 365 nm.

### 2.2. Synthesis

#### 2.2.1. Preparation of sensor TQC

245 mg of 1 mmol compound **1**, 350 mg of 1 mmol compound **2** and 40 mL absolute ethanol was added to 100 mL and heated to reflux for 7 h and TLC monitoring. Then it was cooled to room temperature, filtered, and washed with ice ethanol to afford a yellow solid (550 mg, yield, 95%). mp: >221.4 °C. <sup>1</sup>H NMR (CDCl<sub>3</sub>, 400 MHz,

TMS): δ (ppm) 10.48 (s, 1H, NH), 8.69 (s, 1H, CH=N), 8.53 (s, 1H, ArH), 8.53 (d, 1H, *J* = 8.4 Hz, ArH), 8.40–8.43 (m, 1H, ArH), 8.24 (d, 1H, *J* = 8.4 Hz, ArH), 8.05–8.08 (m, 1H, ArH), 7.45–7.51 (m, 4H, ArH), 7.37 (d, 1H, *J* = 8.8 Hz, ArH), 7.00 (q, 1H, *J* = 2.8 Hz, ArH), 6.62 (dd, 1H, *J*<sub>1</sub> = 8.8 Hz, *J*<sub>2</sub> = 2.4 Hz, ArH), 6.53 (d, 1H, *J* = 2.0 Hz, ArH), 4.83 (s, 2H, COCH<sub>2</sub>O), 3.45 (q, 4H, *J* = 7.2 Hz, CH<sub>2</sub>CH<sub>3</sub>), 1.22–1.26 (m, 6H, CH<sub>3</sub>). <sup>13</sup>C NMR (CDCl<sub>3</sub>, 100 MHz, TMS): δ (ppm): 169.0, 163.7, 161.6, 157.3, 154.1, 152.4, 151.7, 150.7, 144.0, 140.2, 139.3, 136.9, 136.3, 130.6, 130.1, 127.6, 126.3, 126.2, 123.4, 123.3, 121.1, 119.3, 112.3, 110.0, 109.6, 108.8, 97.2, 67.0, 45.1, 12.5. The NMR spectra of sensor TQC were shown in Figs. S1 and S2. HRMS (ESI): *m/z* calcd for C<sub>32</sub>H<sub>28</sub>N<sub>5</sub>O<sub>4</sub>S [(M + H)<sup>+</sup>]: 578.1864, found 578.1858; C<sub>32</sub>H<sub>27</sub>N<sub>5</sub>NaO<sub>4</sub>S [(M + Na)<sup>+</sup>]: 600.1682, found 600.1678 (Fig. S3).

### 2.3. General procedure for UV-vis absorption spectra and fluorescence spectra experiments

All tests were carried out at room temperature (25 °C) in DMSO/HEPES (3:2 v/v, pH = 7.4) buffer system. A stock solution of TQC was prepared (*c* = 1 × 10<sup>-3</sup> M) in DMSO. The stock solutions of various metal ions and anions (1 × 10<sup>-2</sup> M) were prepared from their chloride and sodium salts in deionized water, respectively. The concentration of sensor TQC was 10 μM in all experiments. The UV-vis absorption spectra and fluorescence spectra of sensor TQC at a concentration of 1 × 10<sup>-5</sup> M were recorded at an excitation of 449 nm, the slits of emission and excitation were 5 nm in all experiments. In this study, K<sup>+</sup>, Na<sup>+</sup>, Cs<sup>+</sup>, Li<sup>+</sup>, Ag<sup>+</sup>, Mg<sup>2+</sup>, Ca<sup>2+</sup>, Zn<sup>2+</sup>, Cu<sup>2+</sup>, Hg<sup>2+</sup>, Pb<sup>2+</sup>, Ba<sup>2+</sup>, Cd<sup>2+</sup>, Al<sup>3+</sup>, and Fe<sup>3+</sup> cations and F<sup>-</sup>, Cl<sup>-</sup>, Br<sup>-</sup>, I<sup>-</sup>, HPO<sub>4</sub><sup>2-</sup>, H<sub>2</sub>PO<sub>4</sub><sup>-</sup>, PPI, OAc<sup>-</sup>, HCO<sub>3</sub><sup>-</sup>, CO<sub>3</sub><sup>2-</sup>, HSO<sub>3</sub><sup>-</sup>, SO<sub>3</sub><sup>2-</sup>, SO<sub>4</sub><sup>2-</sup>, S<sup>2-</sup>, NO<sub>3</sub><sup>-</sup> and NO<sub>2</sub><sup>-</sup> anions were tested.

## 2.4. Fluorescence quantum yield experiment

According to formula (3), the relative fluorescence quantum yields were calculated when quinine sulfate ( $\phi = 0.577$ ) was used as the reference solution.

## 2.5. General method for cell imaging

HeLa cells were cultured in culture medium in an in vitro incubator with 5% CO<sub>2</sub> at 37 °C. Cells were seeded onto two culture dishes at a density of  $1.0 \times 10^5$  cells per well and then incubated at 37 °C for 12 h. After washing with PBS (phosphate-buffered saline) buffer two times, the cells were imaged using a fluorescence microscope. Then the cells were incubated with three PBS buffers (containing 5  $\mu$ M sensor **TQC**, 50  $\mu$ M Cu<sup>2+</sup> and 50  $\mu$ M PPI, respectively) for 30 min successively. Each incubation was completed, the dish was washed twice with PBS buffer thoroughly and after that the cells were imaged.

## 3. Results and discussion

### 3.1. The UV-vis recognition

#### 3.1.1. UV-vis recognition of sensor **TQC** toward Cu<sup>2+</sup>

The UV-vis spectrum of sensor **TQC** was recorded in DMSO/HEPES (3:2 v/v, pH = 7.4) and shown in Fig. 1. After the addition (10 equiv.) of various metal ions, namely K<sup>+</sup>, Na<sup>+</sup>, Cs<sup>+</sup>, Li<sup>+</sup>, Ag<sup>+</sup>, Mg<sup>2+</sup>, Ca<sup>2+</sup>, Zn<sup>2+</sup>, Cu<sup>2+</sup>, Hg<sup>2+</sup>, Pb<sup>2+</sup>, Ba<sup>2+</sup>, Cd<sup>2+</sup>, Al<sup>3+</sup>, and Fe<sup>3+</sup>, the presence of Cu<sup>2+</sup> induced a new band at 479 nm with a change in color from bright yellow to orange. The maximum absorption wavelength showed a significant red shift of 30 nm from 449 nm to 479 nm, and the absorbance was also significantly increased, indicating that sensor **TQC** could be used for naked eye recognition of Cu<sup>2+</sup>.

#### 3.1.2. UV-vis titration of sensor **TQC** toward Cu<sup>2+</sup>

As shown in Fig. 2, by successive addition of Cu<sup>2+</sup> ions to sensor **TQC** in DMSO/HEPES (3:2 v/v, pH = 7.4) up to 2.0 equiv., the absorption gradually increased and the maximum absorption wavelength shifted from 449 nm to 479 nm. Further addition of Cu<sup>2+</sup> did not make further significant spectral change. The two isobestic points, observed at 383 nm and 447 nm, indicate that sensor **TQC** and the complex **TQC**-Cu<sup>2+</sup> were in a dynamic equilibrium.

### 3.2. The fluorescence recognition

#### 3.2.1. Fluorescence recognition of sensor **TQC** toward Cu<sup>2+</sup>

The fluorescence response behavior of sensor **TQC** was investigated upon treatment with various metal ions, including K<sup>+</sup>, Na<sup>+</sup>, Cs<sup>+</sup>, Li<sup>+</sup>, Ag<sup>+</sup>, Mg<sup>2+</sup>, Ca<sup>2+</sup>, Zn<sup>2+</sup>, Cu<sup>2+</sup>, Hg<sup>2+</sup>, Pb<sup>2+</sup>, Ba<sup>2+</sup>, Cd<sup>2+</sup>, Al<sup>3+</sup>, and Fe<sup>3+</sup> in DMSO/HEPES (3:2 v/v, pH = 7.4) at an excitation of 449 nm. As shown in Fig. 3, only Cu<sup>2+</sup> led to a remarkable fluorescence quenching at 505 nm ( $\phi$  changed from 0.286 to 0.009), while the other ions caused a little or no fluorescence change. In order to explore the effects of other ions on the recognition of Cu<sup>2+</sup>, the interference tests were carried out. As shown in Fig. S4, the fluorescence intensity of other metal ions solution showed obvious fluorescence quenching after the addition of 10 equiv. of Cu<sup>2+</sup>. Evidently, these metal ions did not interfere with the recognition of Cu<sup>2+</sup>. In consequence, sensor **TQC** showed fine specificity.

#### 3.2.2. Fluorescence titration of sensor **TQC** toward Cu<sup>2+</sup>

The sensitivity of sensor **TQC** for Cu<sup>2+</sup> was investigated by fluorescence titration. The observed changes in the fluorescence emission spectra with Cu<sup>2+</sup> are shown in Fig. 4. The intensity of the fluorescence peak at 505 nm decreased upon successive addition of the Cu<sup>2+</sup> and saturated at 2.0 equiv. and the quenching rate was 100%, indicating that sensor **TQC** was highly sensitive to Cu<sup>2+</sup>. The Job curve at the upper right corner showed that the inflection point was observed at a Cu<sup>2+</sup> concentration of 0.55 equiv., indicating that the coordination ratio of sensor **TQC** and Cu<sup>2+</sup> was 1:1. The complexation constant  $K_a = 6.27 \times 10^4 \text{ M}^{-1}$  ( $Y = 6.43 \times 10^{-9} \times X + 4.03 \times 10^{-4}$ ,  $R^2 = 0.99901$ , Fig. S5). Moreover, the minimum detection limit of sensor **TQC** was calculated to be 0.06  $\mu$ M ( $Y = -918.16 \times X + 1190.88$ ,  $R^2 = 0.99200$ , Fig. S6) by  $\text{LOD} = 3\sigma/m$ , indicating high sensitivity of sensor **TQC**.

#### 3.2.3. Fluorescence recognition of **TQC**-Cu<sup>2+</sup> complex to PPI

The complex formed by sensor **TQC** and Cu<sup>2+</sup> was used as a new sensor **TQC**-Cu<sup>2+</sup> for sequential recognition of anions, including: F<sup>-</sup>, Cl<sup>-</sup>, Br<sup>-</sup>, I<sup>-</sup>, HPO<sub>4</sub><sup>2-</sup>, H<sub>2</sub>PO<sub>4</sub><sup>-</sup>, PPI, OAc<sup>-</sup>, HCO<sub>3</sub><sup>-</sup>, CO<sub>3</sub><sup>2-</sup>, HSO<sub>3</sub><sup>-</sup>, SO<sub>3</sub><sup>2-</sup>, SO<sub>4</sub><sup>2-</sup>, S<sup>2-</sup>, NO<sub>3</sub><sup>-</sup> and NO<sub>2</sub><sup>-</sup>. As shown in Fig. 5, only the addition of PPI instantly caused an obvious fluorescence enhancement but remained unchanged after the addition of other anions. The response rate of H<sub>2</sub>PO<sub>4</sub><sup>-</sup> and HPO<sub>4</sub><sup>2-</sup> was 10% and 12%, respectively. Compared with H<sub>2</sub>PO<sub>4</sub><sup>-</sup> and HPO<sub>4</sub><sup>2-</sup>, the fluorescence was recovered to a large extent after adding PPI with a response rate of above 90% ( $\phi_{\text{recovered}}$  to 0.206), indicating that the new probe could identify PPI specifically. The competitive

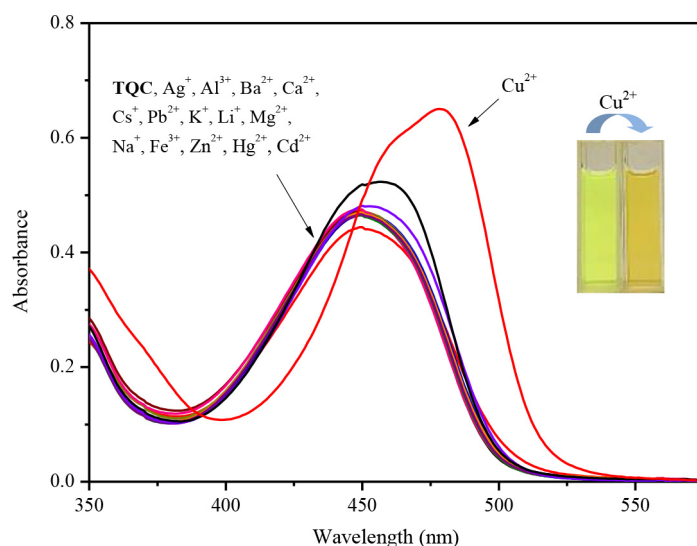


Fig. 1. UV-vis spectra of sensor **TQC** in DMSO/HEPES (3:2 v/v, pH = 7.4) with the addition of 10 equiv. of various metal ions and blank. Inset: the color of sensor **TQC** (10  $\mu$ M) in the absence and presence of Cu<sup>2+</sup> (10 equiv.).

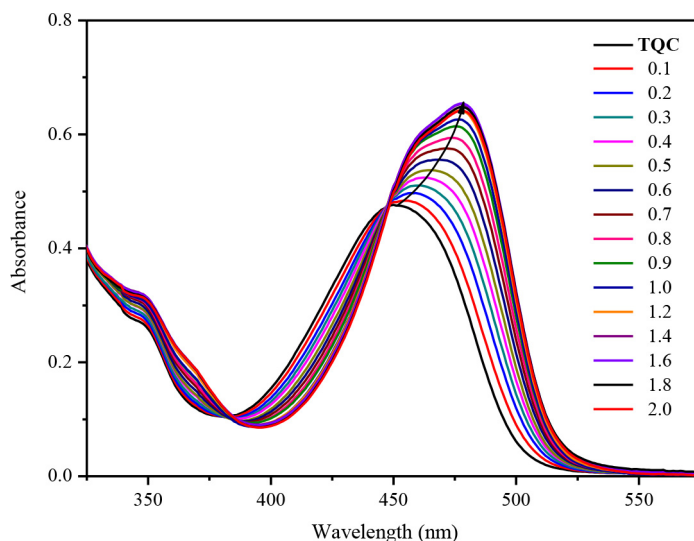


Fig. 2. UV-vis spectra of sensor **TQC** with various concentrations [0–2.0 equiv. of  $\text{Cu}^{2+}$ .] in DMSO/HEPES (3:2 v/v, pH = 7.4).

experiments were further carried out using a solution containing PPI and all other anions. As shown in Fig. S7, the addition of PPI to **TQC**- $\text{Cu}^{2+}$  containing other anions still showing a fluorescent enhancement effect without being interfered by other anions, which further indicated that **TQC**- $\text{Cu}^{2+}$  had good selectivity to PPI among other co-existing anions especially phosphorus-containing anions.

#### 3.2.4. Fluorescence titration of **TQC**- $\text{Cu}^{2+}$ with PPI

As shown in Fig. 6, the intensity of the strongest fluorescence emission peak gradually increased with increasing the PPI concentration up to 10 equiv., after that the intensity remained largely unchanged. Thus, **TQC**- $\text{Cu}^{2+}$  had a high sensitivity to PPI. The job curve at the upper right corner showed that the inflection point was observed at a PPI concentration of 0.3 equiv., indicating that the coordination ratio between probe and PPI was 2:1. Furthermore, the detection limit was  $0.01 \mu\text{M}$  according to the formula  $\text{LOD} = 3\sigma/m$  (Fig. S8).

#### 3.3. Fluorescence lifetime studies

As shown in Fig. 7, the fluorescence lifetime of sensor **TQC** was calculated to be 1.13 ns, when  $\text{Cu}^{2+}$  was added, the fluorescence lifetime shortened to 0.64 ns. Whereas, the addition of PPI resulted in a recovery in fluorescence lifetime which was calculated to be about 1.13 ns, which suggested that sensor **TQC** could be applied for sequential detection of  $\text{Cu}^{2+}$  and PPI.

#### 3.4. Reversibility of sensor **TQC** for $\text{Cu}^{2+}$ and PPI

The stability of sensor **TQC** in identifying  $\text{Cu}^{2+}$  and PPI was discussed with  $\text{Cu}^{2+}$  and PPI as input signals and fluorescence intensity as output signals. As shown in Fig. 8, the fluorescence intensity still remained stable after 6 cycles, indicating that the sensor **TQC** could be used to continuously identify  $\text{Cu}^{2+}$  and PPI in practical applications.

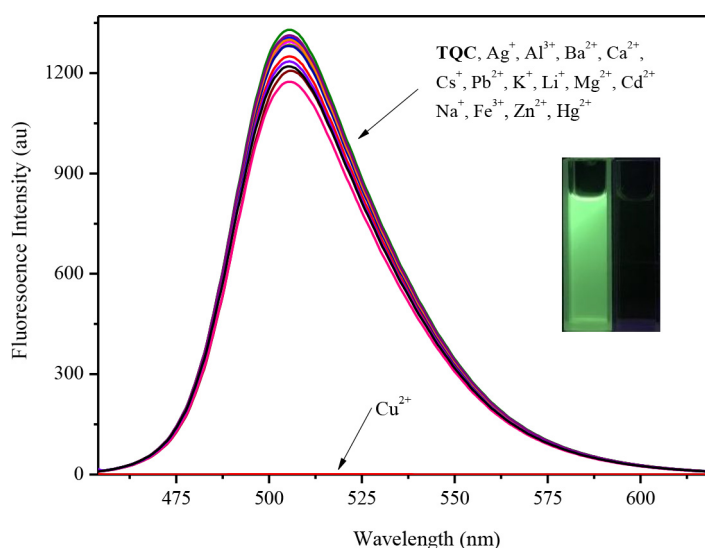
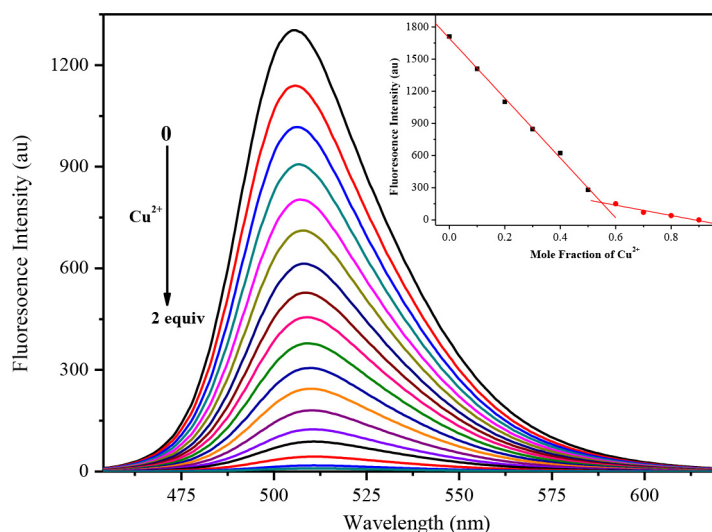


Fig. 3. Fluorescence spectra of sensor **TQC** in DMSO/HEPES (3:2 v/v, pH = 7.4) at an excitation of 449 nm with the addition of 10 equiv. of various metal ion and blank. Inset: the fluorescence of sensor **TQC** (10  $\mu\text{M}$ ) in the absence and presence of  $\text{Cu}^{2+}$  (10 equiv.) under UV light.



**Fig. 4.** Fluorescence spectra of 10  $\mu\text{M}$  sensor **TQC** with the addition of various concentrations [0–2.0 equiv.] of  $\text{Cu}^{2+}$  in DMSO/HEPES (3:2 v/v, pH = 7.4) at an excitation of 449 nm. The inset plots showed that sensor **TQC** formed a 1:1 complex with  $\text{Cu}^{2+}$ .

### 3.5. DFT study

To gain further insight into the photophysical properties and the nature of optical response of sensor **TQC** toward  $\text{Cu}^{2+}$ , **TQC** and **TQC**- $\text{Cu}^{2+}$  were examined by density functional theory calculation by using Gaussian 09 program with the methods of B3LYP/6-31G (d, p) for **TQC** and B3LYP/LANL2DZ for **TQC**- $\text{Cu}^{2+}$ . The optimized structures and the highest occupied molecular orbital (HOMO) and the lowest unoccupied molecular orbital (LUMO) of **TQC** and **TQC**- $\text{Cu}^{2+}$  were shown in Fig. 9. The coumarin ring and the quinolinyl benzothiazole in **TQC** were not in the same plane and presented a dihedral angle of about  $20^\circ$  while were coplanar after complexing with  $\text{Cu}^{2+}$ . Most electrons in the HOMO orbital of **TQC** were located on the coumarin ring. After complexing with  $\text{Cu}^{2+}$ , the electrons transferred toward  $\text{Cu}^{2+}$  and were distributed at the binding site of **TQC** and  $\text{Cu}^{2+}$  and resulted in fluorescence quenching. Meanwhile, the energy gaps between HOMO and LUMO of the **TQC** and **TQC**- $\text{Cu}^{2+}$  were 2.83 eV and 2.64 eV, respectively. It was obvious that the energy gap of **TQC**- $\text{Cu}^{2+}$  was lower than **TQC** which was in accordance with the redshift of **TQC**- $\text{Cu}^{2+}$  in UV-vis absorption. DFT calculations

verified the experimental results and presumed complexation mode of chemosensor **TQC** with  $\text{Cu}^{2+}$  and explained the PET (photo induced electron transfer) process.

### 3.6. The possible mechanism of sensor **TQC** for $\text{Cu}^{2+}$ and PPI

In order to identify the possible mechanism between sensor **TQC** for  $\text{Cu}^{2+}$  and PPI, we did the Job experiment. The Job curves showed that the coordination ratio of sensor **TQC** to  $\text{Cu}^{2+}$  was 1:1 and that to PPI was 2:1. The sensor **TQC** provided six coordination points through O atom and N atom to form a copper complex by 1:1 bonding with  $\text{Cu}^{2+}$ . The coordination complex **TQC**- $\text{Cu}^{2+}$  exhibited a fluorescence quenching response and the probe fluorescence was restored after the addition of PPI. During this process, the sensor fluorescence emission showed no red shift with the increase of  $\text{Cu}^{2+}$  concentration, and it showed a distinct “on-off” fluorescence response. Further efforts were made to study the binding sites of **TQC** with  $\text{Cu}^{2+}$  by means of the ESI-MS spectra (Fig. S10). The molecular ion peak

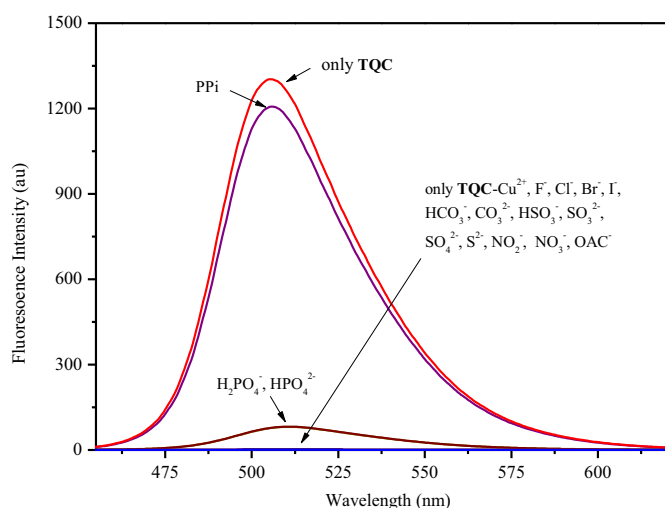


**Fig. 5.** Fluorescence spectra of 10  $\mu\text{M}$  **TQC**- $\text{Cu}^{2+}$  with the addition of 10 equiv. of various anions in DMSO/HEPES (3:2 v/v, pH = 7.4).

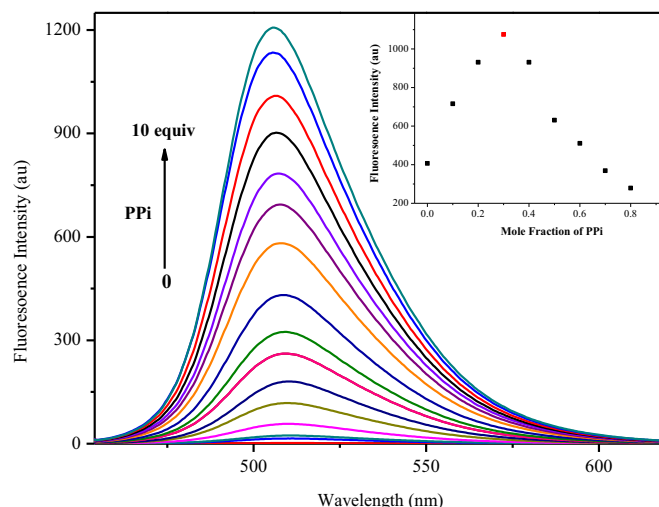


**Fig. 6.** Fluorescence spectra of 10  $\mu\text{M}$  **TQC**- $\text{Cu}^{2+}$  in the presence of various concentrations [0–10 equiv.] of PPI in DMSO/HEPES (3:2 v/v, pH = 7.4) at an excitation of 449 nm. The inset plots indicated that **TQC**- $\text{Cu}^{2+}$  formed a 2:1 complex with PPI.

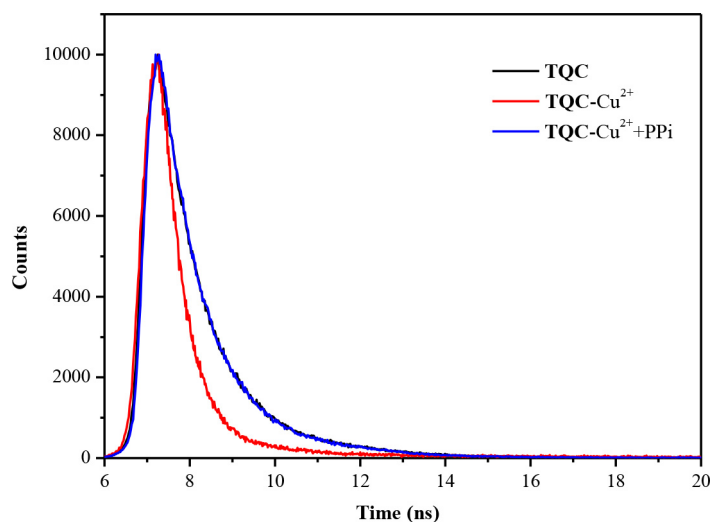


Fig. 7. Transient photoluminescence decay spectra of sensor **TQC** (10  $\mu\text{M}$ ) upon addition of  $\text{Cu}^{2+}$  and PPI in DMSO/HEPES (3:2 v/v, pH = 7.4) buffer system.

(ESI-MS) at 639.09935 [sensor **TQC**- $\text{Cu}^{2+}$ ;  $m/z$  calcd for 639.09905] indicated an 1:1 complexation between sensor **TQC** and  $\text{Cu}^{2+}$ . Based on Job's plot analysis, mass spectrometry, DFT calculation and spectral properties analysis, we speculated that the photoinduced electron transfer from the donor (coumarin rings) to the receptor (quinolinyl-benzothiazole) was blocked at the beginning, then the complexation of  $\text{Cu}^{2+}$  promoted the PET process to occur and caused to quench the fluorescence emission due to the paramagnetic cation of  $\text{Cu}^{2+}$ , and there was no shift of emission spectra. On the contrary, PET process was hindered when  $\text{Cu}^{2+}$  was complexed by PPI and the fluorescence was recovered. So the possible coordination mode was shown in Scheme 2.

### 3.7. Practical application on test strips

A paper strip test was performed as described previously to illustrate its practical utility [47], as shown in Fig. 10. Filter paper strips were put into DMSO/HEPES (3:2 v/v, pH = 7.4) solution of **TQC** for 5 min and dried with paper, and then put into  $\text{Cu}^{2+}$  aqueous solution and PPI aqueous solution in succession and dried again with paper. Obvious

color changes were observed in this process under both visible light and UV irradiation, indicating that the sensor **TQC** had the potential for naked-eye detection of  $\text{Cu}^{2+}$  and PPI in water.

### 3.8. Cell imaging

Fig. S9 showed that the fluorescence at pH = 3–8 was quenched with the addition of  $\text{Cu}^{2+}$  and recovered with the addition of PPI. Because of the excellent selectivity at physiological pH levels, the application of sensor **TQC** for detection of  $\text{Cu}^{2+}$  and PPI in liver cells was further investigated. Fluorescence imaging was performed in HeLa cells, as shown in Fig. 11. No fluorescence was observed in cells (Fig. 11a, a'). Upon the addition of sensor **TQC**, the cells exhibited highly intense green fluorescence (Fig. 11b, b'), indicating that the sensor was well permeable. Cells incubated with  $\text{Cu}^{2+}$  also showed quenching of fluorescence intensity (Fig. 11c, c'). However, fluorescence was restored for cells treated with PPI (Fig. 11d, d'). The cellular studies clearly indicated that sensor **TQC** had great cell permeability and could be supplied as a useful sensor for mapping  $\text{Cu}^{2+}$  and PPI in live cells.

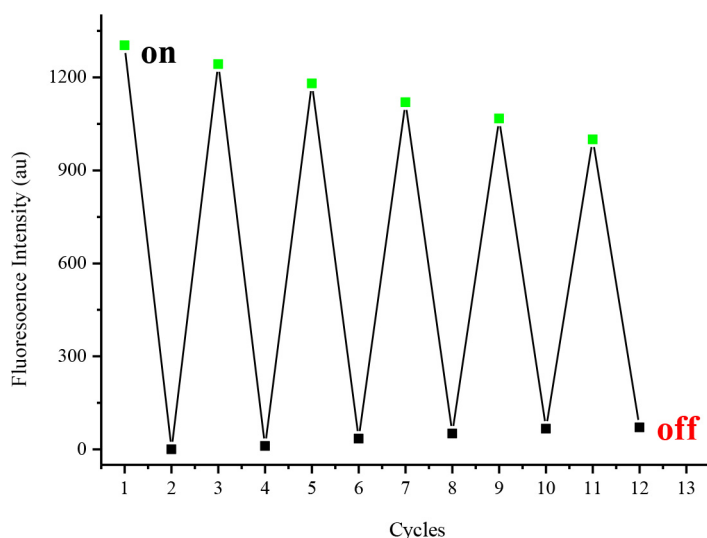
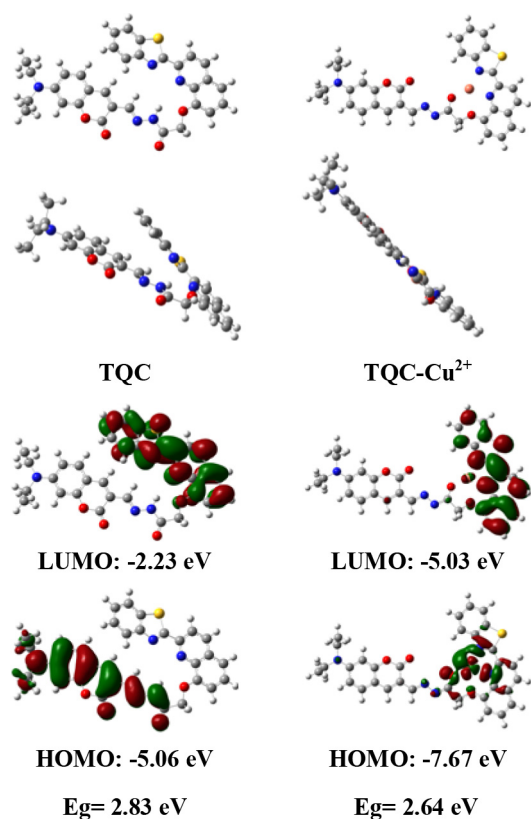


Fig. 8. The sequential reversible behavior of sensor **TQC** (10  $\mu\text{M}$ ) upon alternate addition of  $\text{Cu}^{2+}$  and PPI in DMSO/HEPES (3:2 v/v, pH = 7.4) ( $\lambda_{\text{ex}} = 449 \text{ nm}$ ).



**Fig. 9.** The optimized molecular structure, HOMO and LUMO of **TQC** and **TQC-Cu<sup>2+</sup>** by DFT calculation.

#### 4. Conclusions

In this study, the fluorescent sensor **TQC** was successfully synthesized and its spectral performance for sequential recognition of  $\text{Cu}^{2+}$  and PPI was studied. The sensor **TQC** showed an obvious “on-off-on”

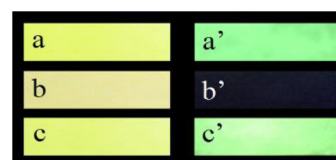


**Fig. 10.** Color changes on test paper in DMSO/HEPES (3:2 v/v, pH = 7.4) (a) **TQC**; (b) **TQC-Cu<sup>2+</sup>**; (c) **TQC-Cu<sup>2+</sup>**+PPI under visible light and (a') **TQC**; (b') **TQC-Cu<sup>2+</sup>**; (c') **TQC-Cu<sup>2+</sup>**+PPI under UV light.

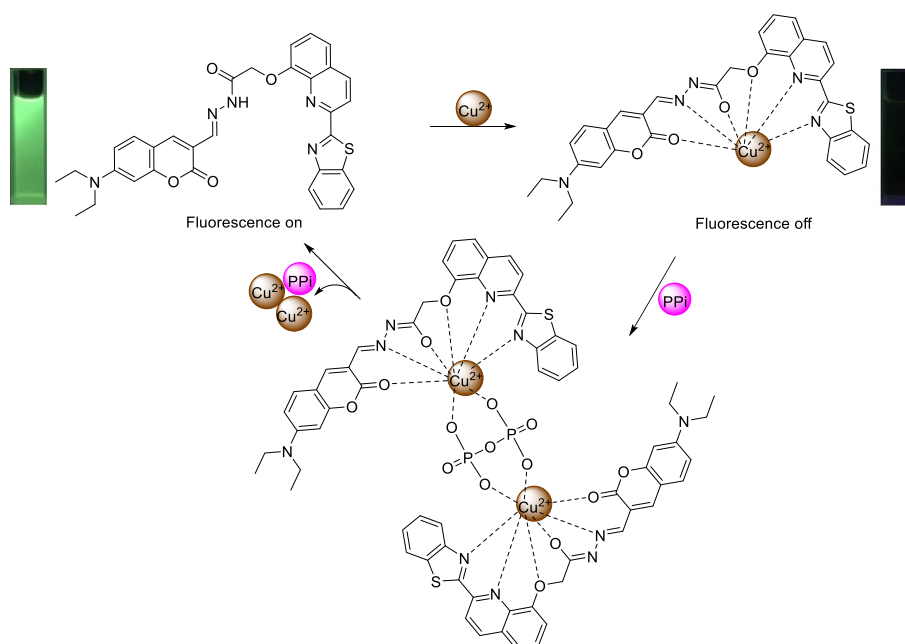
fluorescence response toward  $\text{Cu}^{2+}$  and PPI. The sequential recognition behavior could be repeated six times with little fluorescence efficiency loss using  $\text{Cu}^{2+}$  and PPI. The sensor **TQC** showed a 1:1 binding stoichiometry to  $\text{Cu}^{2+}$  with a complexation constant of  $6.27 \times 10^4 \text{ M}^{-1}$  and the detection limit for  $\text{Cu}^{2+}$  was  $0.06 \mu\text{M}$ . The **TQC-Cu<sup>2+</sup>** complex showed a 2:1 binding stoichiometry to PPI and the detection limit for PPI was calculated to be  $0.01 \mu\text{M}$ . The stable pH range of the sensor **TQC** to  $\text{Cu}^{2+}$  and **TQC-Cu<sup>2+</sup>** to PPI was from 3 to 8. Moreover, the sensor not only could be used to determine  $\text{Cu}^{2+}$  and PPI in test paper strip qualitatively, but also could be successfully applied to detect  $\text{Cu}^{2+}$  and PPI within living cells.

#### CRediT authorship contribution statement

**Shengling Li:**Methodology, Validation, Formal analysis, Investigation, Data curation, Writing - original draft, Writing - review & editing, Project administration.**Duanlin Cao:**Resources, Funding acquisition.**Xianjiao Meng:**Conceptualization.**Zhiyong Hu:**Funding acquisition.**Zhichun Li:**Visualization.**Changchun Yuan:**Resources.**Tao Zhou:**Software, Formal analysis.**Xinghua Han:**Resources.**Wenbing Ma:**Conceptualization, Methodology, Resources, Writing - review & editing, Supervision.

#### Declaration of competing interest

The authors declare that they have no known competing financial interests or personal relationships that could have appeared to influence the work reported in this paper.



**Scheme 2.** The possible mechanism of **TQC-Cu<sup>2+</sup>** with PPI

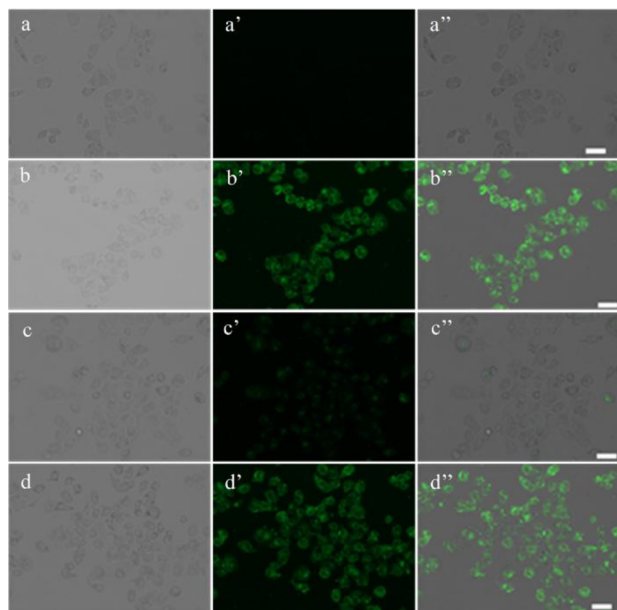


**Fig. 11.** Bright field (a, b, c, d), fluorescence (a', b', c', d') and confocal fluorescence microscope (a'', b'', c'', d'') images of HeLa cells: blank cell (a, a', a''), cells treated with 5  $\mu\text{M}$  TQC (b, b', b''), then treated with 50  $\mu\text{M}$   $\text{Cu}^{2+}$  (c, c', c'') and further treated with 50  $\mu\text{M}$  PPI (d, d', d''). The scale bar was 50  $\mu\text{m}$ .

## Acknowledgements

We gratefully acknowledge the financial support from the Science Foundation of North University of China (No. 110121).

## Appendix A. Supplementary data

Supplementary data includes the  $^1\text{H}$  NMR spectra,  $^{13}\text{C}$  NMR spectra, ESI-MS spectra and part of spectrums of sensor TQC. Supplementary data to this article can be found online at <https://doi.org/10.1016/j.saa.2019.118022>

## References

- Q. Guo, Y. Zhang, Z.H. Lin, Q.Y. Cao, Y. Chen, Fluorescent norbornene for sequential detection of mercury and biothiols, *Dyes Pigments* 172 (2020), 107872. <https://doi.org/10.1016/j.dyepig.2019.107872>.
- K.Q. Fan, X.B. Wang, S.Y. Yu, G.L. Han, D. Xu, L.M. Zhou, J. Song, A chitosan-based fluorescent hydrogel for selective detection of  $\text{Fe}^{2+}$  ions in gel-to-sol mode and turn-off fluorescence mode, *Polym. Chem.* 10 (2019) 5037–5043.
- J. Wang, J. Liang, X. Liu, H. Xiao, F.P. Dong, Y.L. Wang, X. Shu, F.R. Huang, H.B. Liu, Thiazoline-pyrene selective and sensitive fluorescence “turn-on” sensor for detection of  $\text{Cu}^{2+}$ , *Spectrochim. Acta A* 215 (2019) 260–265. <https://doi.org/10.1016/j.saa.2019.02.066>.
- Y.K. Xu, H.Y. Wang, J.Y. Zhao, X.F. Yang, M.S. Pei, G.Y. Zhang, Y.X. Zhang, L. Lin, A simple fluorescent schiff base for sequential detection of  $\text{Zn}^{2+}$  and PPI based on imidazo [2, 1-b] thiazole, *J. Photochem. Photobiol., A* 383 (2019) 112026. <https://doi.org/10.1016/j.jphotochem.2019.112026>.
- W. Zou, F.C. Gong, X.J. Chen, Z. Cao, J.Y. Xia, T.T. Gu, Z.Z. Li, Intrinsically fluorescent and highly functionalized polymer nanoparticles as probes for the detection of zinc and pyrophosphate ions in rabbit serum samples, *Talanta* 188 (2018) 203–209. <https://doi.org/10.1016/j.talanta.2018.05.087>.
- V. Kumar, P. Kumar, S. Kumar, D. Singhal, R. Gupta, Turn-on fluorescent sensors for the selective detection of  $\text{Al}^{3+}$  (and  $\text{Ga}^{3+}$ ) and PPI ions, *Inorg. Chem.* 58 (2019) 10364–10376. <https://doi.org/10.1021/acs.inorgchem.9b01550>.
- S.M. Hwang, M.S. Kim, M. Lee, M.H. Lim, C. Kim, Single fluorescent chemosensor for multiple targets: sequential detection of  $\text{Al}^{3+}$  and pyrophosphate and selective detection of  $\text{F}^-$  in near-perfect aqueous solution, *New J. Chem.* 41 (2017) 15590–15600.
- X.H. Luo, X.Y. Li, Y. Wang, X.M. Xie, L. Yang, A novel reversible fluorescent probe for sequential detection of aluminium ion and PPI and bioimaging in living cells, *ChemistrySelect* 4 (2019) 10643–10648. <https://doi.org/10.1002/slct.201902204>.
- J.H. Choi, A. Pandith, D. Chakradhar, H.R. Kim, H.S. Kim,  $\text{Al}^{3+}$ -Morpholine-appended anthracene ensemble as a dual photonic switch for  $\text{H}_2\text{PO}_4^-$  and  $\text{CN}^-$  ions and its biological applications, *Bull. Kor. Chem. Soc.* 40 (2019) 138–145. <https://doi.org/10.1002/bkcs.11657>.

- W. Wang, M. Wu, H.M. Liu, Q.L. Liu, Y. Gao, B. Zhao, A novel on-off-on fluorescent chemosensor for relay detection of  $\text{Fe}^{3+}$  and PPI in aqueous solution and living cells, *Tetrahedron Lett.* 60 (2019) 1631–1635. <https://doi.org/10.1016/j.tetlet.2019.05.015>.
- X.M. Xu, D.D. Ren, Y.Y. Chai, X. Cheng, J. Mei, J. Bao, F.D. Wei, G.H. Xu, Q. Hu, Y. Cen, Dual-emission carbon dots-based fluorescent probe for ratiometric sensing of Fe (III) and pyrophosphate in biological samples, *Sensors Actuators B Chem.* 298 (2019) 126829. <https://doi.org/10.1016/j.snb.2019.126829>.
- Y.K. Xu, X.G. Liu, J.Y. Zhao, H.Y. Wang, Z. Liu, X.F. Yang, M.S. Pei, G.Y. Zhang, A new “ON-OFF-ON” fluorescent probe for sequential detection of  $\text{Fe}^{3+}$  and PPI based on 2-pyridin-2-yl-ethanamine and benzimidazo [2, 1-a] benz [de] isoquinoline-7-one-12-carboxylic acid, *New J. Chem.* 43 (2019) 474–480.
- Z.A. Li, J. Qiang, J. Li, T.W. Wei, Z.J. Zhang, Y.H. Chen, Q. Kong, F. Wang, X.Q. Chen, Dinuclear Cu (II) complex bearing guanidinium arms for sensing pyrophosphate and monitoring the activity of Ppase, *Dyes Pigments* 163 (2019) 243–248. <https://doi.org/10.1016/j.dyepig.2018.12.004>.
- A. Pandith, K.R. Bhattarai, R.K.G. Siddappa, H.J. Chae, Y.J. Seo, Novel fluorescent C2-symmetric sequential on-off-on switch for  $\text{Cu}^{2+}$  and pyrophosphate and its application in monitoring of endogenous alkaline phosphatase activity, *Sensors Actuators B Chem.* 282 (2019) 730–742. <https://doi.org/10.1016/j.snb.2018.11.111>.
- C.Y. Zhao, J. Chen, D.L. Cao, J.L. Wang, W.B. Ma, Novel coumarin-based containing denrons selective fluorescent chemosensor for sequential recognition of  $\text{Cu}^{2+}$  and PPI, *Tetrahedron* 75 (2019) 1997–2003. <https://doi.org/10.1016/j.tet.2019.02.024>.
- G. Asaithambi, V. Periasamy, Phenanthrene-imidazole-based fluorescent sensor for selective detection of  $\text{Ag}^+$  and  $\text{F}^-$  ions: real sample application and live cell imaging, *Res. Chem. Intermed.* 45 (2019) 1295–1308. <https://doi.org/10.1007/s11164-018-3678-4>.
- S.K. Padhan, J. Palei, P. Rana, N. Murmu, S.N. Sahu, Sequential displacement strategy for selective and highly sensitive detection of  $\text{Zn}^{2+}$ ,  $\text{Hg}^{2+}$  and  $\text{S}^{2-}$  ions: an approach toward a molecular keypad lock, *Spectrochim. Acta A* 208 (2019) 271–284. <https://doi.org/10.1016/j.saa.2018.10.016>.
- F.Q. Bu, B. Zhao, W. Kan, L.M. Ding, T. Liu, L.Y. Wang, B. Song, W.B. Wang, Q.G. Deng, An ESIPt characteristic “turn-on” fluorescence sensor for  $\text{Hg}^{2+}$  with large Stokes shift and sequential “turn-off” detection of  $\text{S}^{2-}$  as well as the application in living cells, *J. Photochem. Photobiol., A* (2019) 112165. <https://doi.org/10.1016/j.jphotochem.2019.112165>.
- J.J. Xuan, J.T. Tian, Heating promoted fluorescent recognition of  $\text{Cu}^{2+}$  with high selectivity and sensitivity based on spiro-pyran derivative, *Anal. Chim. Acta* 1061 (2019) 161–168. <https://doi.org/10.1016/j.aca.2019.02.028>.
- J.B. Xu, N. Liu, C.W. Hao, Q.Q. Han, Y.L. Duan, J. Wu, A novel fluorescence “on-off-on” peptide-based chemosensor for simultaneous detection of  $\text{Cu}^{2+}$ ,  $\text{Ag}^+$  and  $\text{S}^{2-}$ , *Sensors Actuators B Chem.* 280 (2019) 129–137. <https://doi.org/10.1016/j.snb.2018.10.038>.
- H.Q. Li, X.Q. Sun, T.X. Zheng, Y.X. Song, X.H. Gu, Coumarin-based multifunctional chemosensor for arginine/lysine and  $\text{Cu}^{2+}/\text{Al}^{3+}$  ions and its  $\text{Cu}^{2+}$  complex as colorimetric and fluorescent sensor for biothiols, *Sensors Actuators B Chem.* 279 (2019) 400–409. <https://doi.org/10.1016/j.snb.2018.10.017>.
- X.J. Meng, S.L. Li, W.B. Ma, J.L. Wang, Z.Y. Hu, D.L. Cao, Highly sensitive and selective chemosensor for  $\text{Cu}^{2+}$  and  $\text{H}_2\text{PO}_4^-$  based on coumarin fluorophore, *Dyes Pigments* 154 (2018) 194–198. <https://doi.org/10.1016/j.dyepig.2018.03.002>.
- B. Zhang, Q.P. Diao, P.Y. Ma, X. Liu, D.Q. Song, X.H. Wang, A sensitive fluorescent probe for  $\text{Cu}^{2+}$  based on rhodamine B derivatives and its application to drinking water examination and living cells imaging, *Sensors Actuators B Chem.* 225 (2016) 579–585. <https://doi.org/10.1016/j.snb.2015.11.069>.
- S. Slassi, M. Aarjane, A. El-Ghayoury, A. Amine, A highly turn-on fluorescent CHEF-type chemosensor for selective detection of  $\text{Cu}^{2+}$  in aqueous media, *Spectrochim. Acta A* 215 (2019) 348–353. <https://doi.org/10.1016/j.saa.2019.02.099>.
- S. Zeng, S.J. Li, X.J. Sun, T.T. Liu, Z.Y. Xing, A dual-functional chemosensor for fluorescent on-off and ratiometric detection of  $\text{Cu}^{2+}$  and  $\text{Hg}^{2+}$  and its application in cell imaging, *Dyes Pigments* (2019), 107642. <https://doi.org/10.1016/j.dyepig.2019.107642>.
- F. Shi, S.Q. Cui, H.L. Liu, S.Z. Pu, A high selective fluorescent sensor for  $\text{Cu}^{2+}$  in solution and test paper strips, *Dyes Pigments* (2019) 107914. <https://doi.org/10.1016/j.dyepig.2019.107914>.
- Y. Feng, Y. Yang, Y.Z. Wang, F.Z. Qiu, X.R. Song, X.L. Tang, G.L. Zhang, W.S. Liu, Dual-functional colorimetric fluorescent probe for sequential  $\text{Cu}^{2+}$  and  $\text{S}^{2-}$  detection in bio-imaging, *Sensors Actuators B Chem.* 288 (2019) 27–37. <https://doi.org/10.1016/j.snb.2019.02.062>.
- Z. Liu, L.J. Liu, J.L. Li, Y.Y. Qin, C.Y. Zhao, Y. Mi, G.P. Li, T.S. Li, Y.G. Wu, A new coumarin-based fluorescent probe for selective recognition of  $\text{Cu}^{2+}$  and  $\text{S}^{2-}$  in aqueous solution and living cells, *Tetrahedron* 75 (2019) 3951–3957. <https://doi.org/10.1016/j.tet.2019.05.057>.
- J.Z. Li, T.H. Leng, Z.Q. Wang, L. Zhou, X.Q. Gong, Y.J. Shen, C.Y. Wang, A large Stokes shift, sequential, colorimetric fluorescent probe for sensing  $\text{Cu}^{2+}/\text{S}^{2-}$  and its applications, *J. Photochem. Photobiol., A* 373 (2019) 146–153. <https://doi.org/10.1016/j.jphotochem.2019.01.006>.
- X. Wang, P. Xia, X.H. Huang, A dansyl-appended N-heterocycle for  $\text{Cu}^{2+}$  and  $\text{S}^{2-}$  recognition via a displacement mode, *Spectrochim. Acta A* 210 (2019) 98–104. <https://doi.org/10.1016/j.saa.2018.11.017>.
- W.J. Qu, G.T. Yan, X.L. Ma, T.B. Wei, Q. Lin, H. Yao, Y.M. Zhang, “Cascade recognition” of  $\text{Cu}^{2+}$  and  $\text{H}_2\text{PO}_4^-$  with high sensitivity and selectivity in aqueous media based on the effect of ESIPt, *Sensors Actuators B Chem.* 242 (2017) 849–856. <https://doi.org/10.1016/j.snb.2016.09.173>.
- Y.L. Fu, C.B. Fan, G. Liu, S.Z. Pu, A colorimetric and fluorescent sensor for  $\text{Cu}^{2+}$  and  $\text{F}^-$  based on a diarylethene with a 1, 8-naphthalimide Schiff base unit, *Sensors Actuators B Chem.* 239 (2017) 295–303. <https://doi.org/10.1016/j.snb.2016.08.020>.

- [33] Z.Y. Xu, H. Wang, Z. Chen, H.L. Jiang, Y.Q. Ge, Spectrochim. Near-infrared fluorescent probe for selective detection of  $\text{Cu}^{2+}$  in living cells and in vivo, *Acta, Part A* 216 (2019) 404–410, <https://doi.org/10.1016/j.saa.2019.03.062>.
- [34] X.C. Xu, X.B. Zou, S.W. Wu, L.J. Wang, X.H. Niu, X. Li, J.M. Pan, H.L. Zhao, M.B. Lan, In situ formation of fluorescent polydopamine catalyzed by peroxidase-mimicking FeCo-LDH for pyrophosphate ion and pyrophosphatase activity detection, *Anal. Chim. Acta* 1053 (2019) 89–97, <https://doi.org/10.1016/j.aca.2018.12.006>.
- [35] C. Li, Y. Chen, L.J. Yang, C.R. Zhang, B. Wang, Y. Wang, Sens. Tetraphenylethene decorated hyperbranched poly (amido amine)s as metal/organic-solvent-free turn-on AIE probe for specific pyrophosphate detection, *Actuators, B* 291 (2019) 25–33, <https://doi.org/10.1016/j.snb.2019.04.056>.
- [36] D. Liu, S. Liu, X.Y. Zhang, Q. Zhang, J.H. Yu, M.D. Yang, X.Y. Yang, Y.P. Tian, X.J. Zhu, H.P. Zhou, A water-soluble benzoxazole-based probe: real-time monitoring PPI via situ reaction by two-photon cells imaging, *Talanta* 195 (2019) 158–164, <https://doi.org/10.1016/j.talanta.2018.11.036>.
- [37] X.L. Jin, X.L. Wu, B. Wang, P. Xie, Y.L. He, H.W. Zhou, B. Yan, J.J. Yang, W.X. Chen, X.H. Zhang, A reversible fluorescent probe for  $\text{Zn}^{2+}$  and ATP in living cells and in vivo, *Sensors Actuators B Chem.* 261 (2018) 127–134, <https://doi.org/10.1016/j.snb.2018.01.116>.
- [38] M.J. Chang, M.H. Lee, A highly selective dual-channel fluorescent probe for the detection of  $\text{Zn}^{2+}$  ion and pyrophosphate in micelle, *Dyes Pigments* 149 (2018) 915–920, <https://doi.org/10.1016/j.dyepig.2017.11.057>.
- [39] W.J. Zhang, S.G. Liu, L. Han, H.Q. Luo, N.B. Li, Sens. A ratiometric fluorescent and colorimetric dual-signal sensing platform based on N-doped carbon dots for selective and sensitive detection of copper (II) and pyrophosphate ion, *Sensors Actuators B Chem.* 283 (2019) 215–221, <https://doi.org/10.1016/j.snb.2018.12.012>.
- [40] N.B. Azaza, S. Elleuch, S. Khemakhem, Y. Abid, H. Ammar, Synthesis and spectral properties of coumarins derivatives fluorescence emitters: experiment and DFT/TDDFT calculations, *Opt. Mater.* 83 (2018) 138–144, <https://doi.org/10.1016/j.optmat.2018.05.082>.
- [41] S. Zeng, S.J. Li, X.J. Sun, M.Q. Li, Z.Y. Xing, J.L. Li, A benzothiazole-based chemosensor for significant fluorescent turn-on and ratiometric detection of  $\text{Al}^{3+}$  and its application in cell imaging, *Inorg. Chim. Acta* 486 (2019) 654–662, <https://doi.org/10.1016/j.ica.2018.11.042>.
- [42] Z.N. Lu, L. Wang, X. Zhang, Z.J. Zhu, A selective fluorescent chemosensor for  $\text{Cd}^{2+}$  based on 8-hydroxyquinoline-benzothiazole conjugate and imaging application, *Spectrochim. Acta A* 213 (2019) 57–63, <https://doi.org/10.1016/j.saa.2019.01.041>.
- [43] Z.P. Zhang, J.Y. Feng, P.C. Huang, S. Li, F.Y. Wu, Ratiometric fluorescent detection of phosphate in human serum with functionalized gold nanoclusters based on chelation-enhanced fluorescence, *Sensors Actuators B Chem.* 298 (2019) 126891, <https://doi.org/10.1016/j.snb.2019.126891>.
- [44] Q.P. Qin, S.L. Wang, M.X. Tan, Y.C. Liu, T. Meng, B.Q. Zou, H. Liang, Synthesis of two platinum (II) complexes with 2-methyl-8-quinolinol derivatives as ligands and study of their antitumor activities, *Eur. J. Med. Chem.* 161 (2019) 334–342, <https://doi.org/10.1016/j.ejmech.2018.10.051>.
- [45] J.S. Wu, W.M. Liu, X.Q. Zhuang, F. Wang, P.F. Wang, S.L. Tao, X.H. Zhang, S.K. Wu, S.T. Lee, Fluorescence turn on of coumarin derivatives by metal cations: a new signaling mechanism based on C=N isomerization, *Org. Lett.* 9 (2007) 33–36.
- [46] K. Aich, S. Goswami, S. Das, C.D. Mukhopadhyay, C.K. Quah, H.K. Fun,  $\text{Cd}^{2+}$  triggered the FRET “ON”: a new molecular switch for the ratiometric detection of  $\text{Cd}^{2+}$  with live-cell imaging and bound X-ray structure, *Inorg. Chem.* 54 (2015) 7309–7315, <https://doi.org/10.1021/acs.inorgchem.5b00784>.
- [47] A. Roy, S. Dey, P. Roy, A ratiometric chemosensor for  $\text{Al}^{3+}$  based on naphthalene-quinoline conjugate with the resultant complex as secondary sensor for  $\text{F}^{-}$ : interpretation of molecular logic gates, *Sensors Actuators B Chem.* 237 (2016) 628–642, <https://doi.org/10.1016/j.snb.2016.06.139>.